The Effect of Cloud Size Distribution on Direct Entrainment and Detrainment in LES of Shallow Convection

TIBERIU V. POPA* AND PHILIP H. AUSTIN

Department of Earth, Ocean and Atmospheric Sciences
University of British Columbia

1. Introduction

Biases in the parameterization of subgrid-scale shallow cumulus fluxes in general circulation model (GCM) simulations are the dominant source of inter-model variance in climate sensitivity estimates of the cloud radiative response (e.g. Bony and Dufresne 2005; Williams and Webb 2009). Entrainment of environmental properties into clouds and detrainment of cloud properties into the environment largely determine the characteristics of shallow cumulus fields (Sanderson et al. 2008; Klocke et al. 2011), therefore an understanding of the controls on entrainment and detrainment is requisite to accurately model global climate.

Entrainment and detrainment parameterizations proposed in the literature use a wide range of predictive variables spanning cloud morphological parameters: surface area, cross-sectional area a, radius, cloud-top height (e.g. Tiedtke 1989; Bretherton and Park 2009); buoyancy sorting parameters: critical mixing fraction χ_c (the fraction of environmental air required to render a cloudy mixture neutrally buoyant, e.g. Bretherton et al. 2004; de Rooy and Siebesma 2008); and dynamic variables: vertical velocity w, buoyancy B and their lapse rates (e.g. Neggers et al. 2002; Gregory 2001; von Salzen and McFarlane 2002). Such parameterizations have often been tested against Large Eddy Simulation (LES) using mean cloud field tracer budgets (e.g. Siebesma and Cuijpers 1995) without consensus regarding the best predictors of entrainment and detrainment emerging in the modeling community.

More recently, Dawe and Austin (2013) have calculated the relationship between fractional entrainment/detrainment and a variety of mean cloud core and environmental properties for individual shallow cumulus clouds from two standard simulations of the Global Energy and Water Cycle Experiment (GEWEX) Cloud System Studies (GCSS, Randall et al. 2003) using subgrid-scale interpolation to obtain a direct measurement of entrainment and detrainment from LES as described in Dawe and Austin (2011), with the cloud tracking algorithm of Dawe and Austin (2012) used to follow clouds over their lifecycle. Their work suggests that the fractional entrainment rate ε is most closely related to the mean cloud buoyancy B and the environmental buoyancy lapse rate $d\overline{\theta_\rho}/dz$ at that level, while the fractional detrainment δ correlates most closely with the mean cloud vertical velocity w and the critical mixing fraction χ_c at that level. To examine these relationships over a broader range of cloud and environmental conditions, we construct a family of simulations spanning a range of cloud size distributions for non-precipitating and precipitating clouds controlled by the large-scale boundary conditions and external advective and radiative forcings.

2. Model Description and Output Data Sets

All LES calculations were made using the System for Atmospheric Modeling (SAM, Khairoutdinov and Randall 2003). The large-eddy simulations are based on the Cloud Feedbacks Model Intercomparison Project (CFMIP) Global Atmospheric Systems Studies (GASS) Intercomparison of Large Eddy and Single Column Models (CGILS) trade cumulus control case (S6) of Blossey et al. (2013), typified by cloud tops below 3 km and cloud fractions of less than 10%. Quasi-steady state shallow cumulus regimes with a range of cloud size distributions are generated by setting sea-surface temperature (SST) at 298.76 K (CGILS S6), 300 K and 301 K and balancing large-scale subsidence warming and radiative cooling using the framework of Bellon and Stevens (2012), which minimizes the number of parameters used to control the shallow cumulus regimes.

The simulations were performed on a 9.6 km×9.6 km horizontal×4.8 km vertical domain for 48 hours, using a 25 m grid size in all directions and a 1 second time step. The CGILS S6 control simulation required 10 days

*Corresponding author address: Tiberiu V. Popa, Department of Earth, Ocean, and Atmospheric Sciences, University of British Columbia, Room 2020, Earth Sciences Building, 2207 Main Mall, Vancouver, BC, V6T 1Z4, Canada
E-mail: vladpopa@eos.ubc.ca

of model time to attain quasi-steady state, while the perturbed simulations required 48 hours of model time to reach quasi-steady state when initialized with the CGILS S6 control simulation turbulent boundary layer. For all simulations, cloud base is at approximately 550 m, while maximum cloud depth is 2375 m for the CGILS S6 control case, 2775 m for the 300 K SST case and 3300 m for the 301 K SST case. Instantaneous model fields were output each minute and individual cloud histories obtained using the cloud tracking algorithm of Dawe and Austin (2012) identified 9522 clouds, resulting in 56,198 cloud snapshots comprising a total of over 2.6×10^5 samples of cloud properties at various heights and times.

3. Entrainment and Detrainment in the CGILS Simulations

Figure 1 shows the distribution of cloud depth d for the three simulations. The probability distribution functions (PDFs) follow power law scalings when binned using either the horizontal cloud scale l determined as the square root of cloud horizontal area a at height z or the individual cloud depth d as a measure of cloud size. The distributions show a scale break in the vicinity of d = 1000 m. We use d to categorize clouds as either "small" ($d <$ 1000 m) or "large" ($d >$ 1000 m). Below we examine the variation of entrainment rate E (the horizontal convergence of mass into the cloud, $\mathrm{kg\,m^{-3}\,s^{-1}}$), the vertical mass flux M ($\mathrm{kg\,m^{-2}\,s^{-1}}$) and the fractional entrainment rate $\varepsilon = E/M$ ($\mathrm{m^{-1}}$) as a function of cloud size and environmental and cloud characteristics; we similarly examine the related quantities describing the horizontal divergence of mass out of the cloud: detrainment rate D and fractional detrainment rate δ.

The dependence of the entrainment rate E on cloud size is shown in Figure 2. We omit the histograms of $M(l)$ which fit well with a power law of the form $M(l) = M_0 l^m$ with exponent m in the range 2.43 to 2.72. We aim to find a similar power law relationship between cloud size and fractional entrainment rate $\varepsilon = \varepsilon_0 l^e$, but this is difficult to determine directly due to the greater variability in ε than either M or E caused by large values of ε for clouds with near-zero mass flux. Instead we proceed indirectly by fitting $E = M\varepsilon = M_0\varepsilon_0 l^{m-e}$, which produces the values for the exponent $m-e$ between 1.9–2.0 in Figure 2 a, b and c. Combined with the estimate of $m \approx 2.5$, this gives $e \approx 0.5$ as shown in the height-dependent plots of Figure 2.

Joint PDFs between $\log_{10}(\varepsilon)$ and cloud core properties (vertical velocity w, cloud core horizontal area a, buoyancy B, relative humidity RH of the non-cloudy model grid cells that are nearest-neighbour adjacent to cloudy cells or the "cloud shell", and the height z) are calculated to determine the dependence of the fractional mass entrainment rate ε on cloud variables. As shown in the first column of Figure 3, there is little variation in fractional entrainment rate across a wide range of cloud sizes, consistent with the relatively small exponent e found in Figure 2. As in Dawe and Austin (2012), larger variable values are associated with smaller $\log_{10}(\varepsilon)$ for w and B and with larger values of $\log_{10}(\varepsilon)$ for cloud shell RH across the CGILS simulations (not shown), as well as for the cloud scale bins of "small" clouds (Figure 3) and "large" clouds (not shown). Similar relationships are observed from the joint PDFs of the $\log_{10}$ of the fractional detrainment rate δ (not shown).

We calculate the mutual information (MI, Shannon and Weaver 1949; Dawe and Austin 2013) between entrainment/detrainment and cloud properties using PDFs determined from histograms to quantify the strength of the qualitative dependencies suggested by the joint PDFs and to untangle the strong correlations between cloud properties reported by Dawe and Austin (2012). Conditional MI is used to rank the strength of the relationships between entrainment/detrainment and multiple cloud properties. Average cloud buoyancy B consistently shares the highest MI with ε across the CGILS simulations, as well as across the cloud scale bins, while vertical velocity w shares the highest MI with ε conditional on B in most cases. No cloud property showed a significant conditional MI for the 301 K SST case, while the lapse rate of environmental density potential temperature $d\overline{\theta_\rho}/dz$ shared the largest MI with ε conditional on w for the clouds with depth $d >$ 1000 m. Vertical velocity w consistently shared the highest MI with δ across the CGILS simulations, as well as across cloud scale bins, with $d\overline{\theta_\rho}/dz$ sharing the highest MI with δ conditional on w in most cases, although this was not always statistically significant.

We attempt to infer the functional form of the relationships suggested by the MI analysis by fitting power laws between ε, δ and the cloud properties with the highest predictive power as indicated by the MI. Power law relationships between $\log_{10}(\varepsilon)$ and predictors $\log_{10}(B)$, $\log_{10}(w)$ and $\log_{10}(Bw)$ obtained by performing linear least-squares best fits for the clouds with $d <$ 1000 m (Figure 4) suggest a close-to-inverse relationship (slope of -0.86) between $\log_{10}(\varepsilon)$ and $\log_{10}(Bw)$, as well as yielding the lowest RMS error. When all tracked clouds are considered, the relationship between $\log_{10}(\varepsilon)$ and $\log_{10}(Bw)$ results in the lowest RMS error (slope of -0.77, not shown), while for the clouds with $d >$ 1000 m, the relationship between $\log_{10}(\varepsilon)$ and $\log_{10}(wd\overline{\theta_\rho}/dz)$ results in the lowest RMS error (slope of -0.89, not shown).

Power law relationships between $\log_{10}(\delta)$ and predictors $\log_{10}(w)$, $\log_{10}(d\overline{\theta_\rho}/dz)$ and $\log_{10}(wd\overline{\theta_\rho}/dz)$ show lowest variance for the relationship between $\log_{10}(\delta)$ and $\log_{10}(w)$, with slopes of -1.34 for all tracked clouds, -1.39 for clouds with depth $d <$ 1000 m and -1.36 for clouds with depth $d >$ 1000 m (not shown).

4. Discussion

Previous work by Dawe and Austin (2013) determined the joint PDFs for cloud core fractional mass entrainment/detrainment rates and horizontal mean cloud core properties, as well as empirical best-fit relations between entrainment/detrainment and measures of cloud buoyancy, environmental moisture and stability in cloud populations of the simulated BOMEX (ocean equilibrium) and ARM (land diurnal cycle) LES datasets. We extend this work by verifying these relationships using a family of quasi-steady state CGILS-based cloud fields.

Using MI analysis we determine the cloud variables that correlate most closely to fractional entrainment ε and confirm the findings of Dawe and Austin (2012), namely that at all heights in individual clouds average cloud buoyancy B is most closely related to ε, followed by the lapse rate of environmental density potential temperature $d\overline{\theta_\rho}/dz$ for the clouds with depth $d > 1000$ m. In contrast to Dawe and Austin (2012), we find that at all heights in individual clouds vertical velocity w is more strongly related to ε than $d\overline{\theta_\rho}/dz$ for the clouds with depth $d < 1000$, as well as for the individual clouds in the three CGILS-based simulations; the latter is likely due to the large number of "small" clouds. Vertical velocity w at all heights in individual clouds is most related to δ across all CGILS-based simulations and cloud size bins, confirming the findings of Dawe and Austin (2012). However, we find no evidence that the critical mixing fraction χ_c or the cloud shell RH are closely correlated with δ in the CGILS simulations. For all cloud properties considered, their functional relationships to ε and δ appear tantalizingly close to inverse relationships.

Finally, we find power law relationships relating cloud vertical mass flux distribution $M(l) = M_0 l^{2.5}$ and entrainment rate $E(l) = E_0 l^{0.5}$ to cloud horizontal scale l at all heights in individual clouds that are robust across the CGILS-based simulations controlled by SST, as well as across cloud size bins.

References

Bellon, G. and B. Stevens, 2012: Using the sensitivity of large-eddy simulations to evaluate atmospheric boundary layer models. *J. Atmos. Sci.*, **69 (5)**, 1582–1601, doi:10.1175/JAS-D-11-0160.1.

Blossey, P. N., et al., 2013: Marine low cloud sensitivity to an idealized climate change: the CGILS LES intercomparison. *J. Adv. Model. Earth Syst.*, **5 (2)**, 234–258, doi:10.1002/jame.20025.

Bony, S. and J. Dufresne, 2005: Marine boundary layer clouds at the heart of tropical cloud feedback uncertainties in climate models. *Geophys. Res. Let.*, **32 (20)**, L20 806, doi:10.1029/2005GL023851.

Bretherton, C. S., J. R. McCaa, and H. Grenier, 2004: A new parameterization for shallow cumulus convection and its application to marine subtropical cloud-topped boundary layers. part i: description and 1d results. *Mon. Wea. Rev.*, **132**, 864–882, doi:10.1175/1520-0493(2004)132⟨0883:ANPFSC⟩2.0.CO;2.

Bretherton, C. S. and S. Park, 2009: A New Moist Turbulence Parameterization in the Community Atmosphere Model. *J. Climate*, **22 (12)**, 3422–3448, doi:10.1175/2008JCLI2556.1.

Dawe, J. T. and P. H. Austin, 2011: Interpolation of LES cloud surfaces for use in direct calculations of entrainment and detrainment. *Mon. Wea. Rev.*, **139 (2)**, 444–456, doi:10.1175/2010MWR3473.1.

Dawe, J. T. and P. H. Austin, 2012: Statistical analysis of an LES shallow cumulus cloud ensemble using a cloud tracking algorithm. *Atmos. Chem. Phys.*, **12 (2)**, 1101–1119, doi:10.5194/acp-12-1101-2012.

Dawe, J. T. and P. H. Austin, 2013: Direct entrainment and detrainment rate distributions of individual shallow cumulus clouds in an LES. *Atmos. Chem. Phys. Discuss.*, **13 (2)**, 5365–5410, doi:10.5194/acpd-13-5365-2013.

de Rooy, W. C. and A. P. Siebesma, 2008: A simple parameterization for detrainment in shallow cumulus. *Mon. Wea. Rev.*, **136**, 560–576.

Gregory, D., 2001: Estimation of entrainment rate in simple models of convective clouds. *Q. J. R. Meteorol. Soc.*, **127 (571, Part A)**, 53–72.

Khairoutdinov, M. F. and D. A. Randall, 2003: Cloud resolving modeling of the ARM summer 1997 IOP: model formulation, results, uncertainties, and sensitivities. *J. Atmos. Sci.*, **60**, 607–625.

Klocke, D., R. Pincus, and J. Quaas, 2011: On constraining estimates of climate sensitivity with present-day observations through model weighting. *J. Climate*, **24**, 6092–6099, doi:10.1175/2011JCLI4193.1.

Neggers, R. A. J., A. P. Siebesma, and H. J. J. Jonker, 2002: A multiparcel model for shallow cumulus convection. *J. Atmos. Sci.*, **59**, 1655–1668.

Randall, D., et al., 2003: Confronting models with data: the GEWEX cloud systems study. *Bulletin of the American Meteorological Society*, **84 (4)**, 455–469, doi:10.1175/BAMS-84-4-455.

Sanderson, B. M., et al., 2008: Constraints on model response to greenhouse gas forcing and the rold of subgrid-scale processes. *J. Climate*, **21**, 2384–2400, doi:10.1175/2008JCLI1869.1.

Shannon, C. E. and W. Weaver, 1949: *The Mathematical Theory of Communication*. University of Illinois Press.

Siebesma, A. P. and J. W. M. Cuijpers, 1995: Evaluation of parametric assumptions for shallow cumulus convection. *J. Atmos. Sci.*, **52**, 650–666.

Tiedtke, M., 1989: A comprehensive mass flux scheme for cumulus parameterization in large-scale models. *Mon. Wea. Rev.*, **117**, 1779–1800.

von Salzen, K. and N. A. McFarlane, 2002: Parameterization of the bulk effects of lateral and cloud-top entrainment in transient shallow cumulus clouds. *J. Atmos. Sci.*, **59**, 1405–1430, doi:10.1175/1520-0469(2002)059⟨1405:POTBEO⟩2.0.CO;2.

Williams, K. D. and M. J. Webb, 2009: A quantitative performance assessment of cloud regimes in climate models. *Clim. Dyn.*, **33 (1)**, 141–157, doi:10.1007/s00382-008-0443-1.

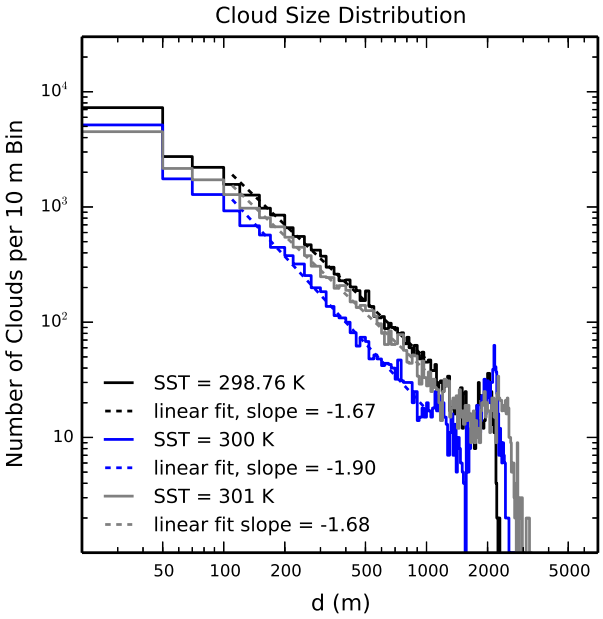

FIG. 1. Histograms of cloud vertical scale d calculated from CGILS-based simulations with SST of 298.76 K (CGILS S6, black line), 300 K (blue line) and 301 K (grey line) using a 10 m bin width. The dashed lines show linear best fit between 100-1000 m length scales to the cloud histograms.

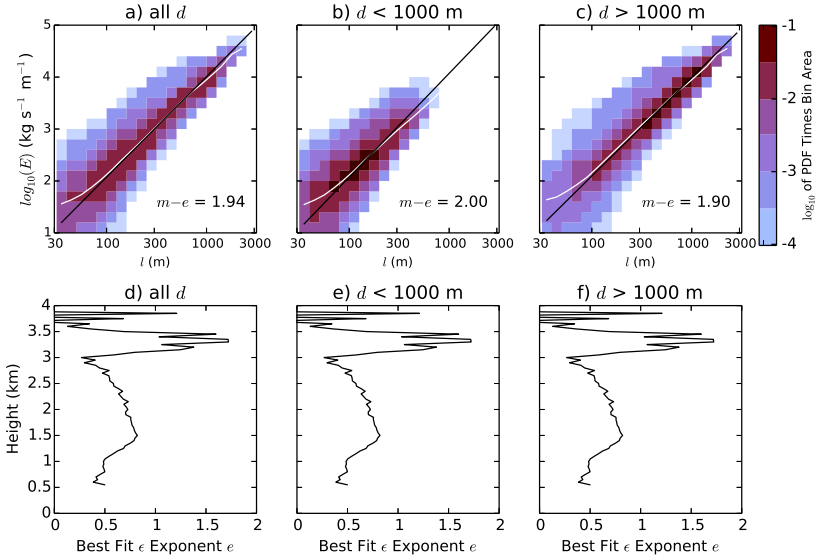

FIG. 2. Power law fits for mass entrainment rate E versus cloud horizontal scale l. a) and d) are calculated from all CGILS clouds; b) and e) from clouds with thickness $d < 1000$ m and c) and f) from clouds with thickness $d > 1000$ m. a), b) and c) show fits based upon data from all heights; white lines show mean E at each l, black lines show the best-fit power law. d), e) and f) show fractional entrainment rate ε power law fit exponent e as a function of height in 50 meter bins.

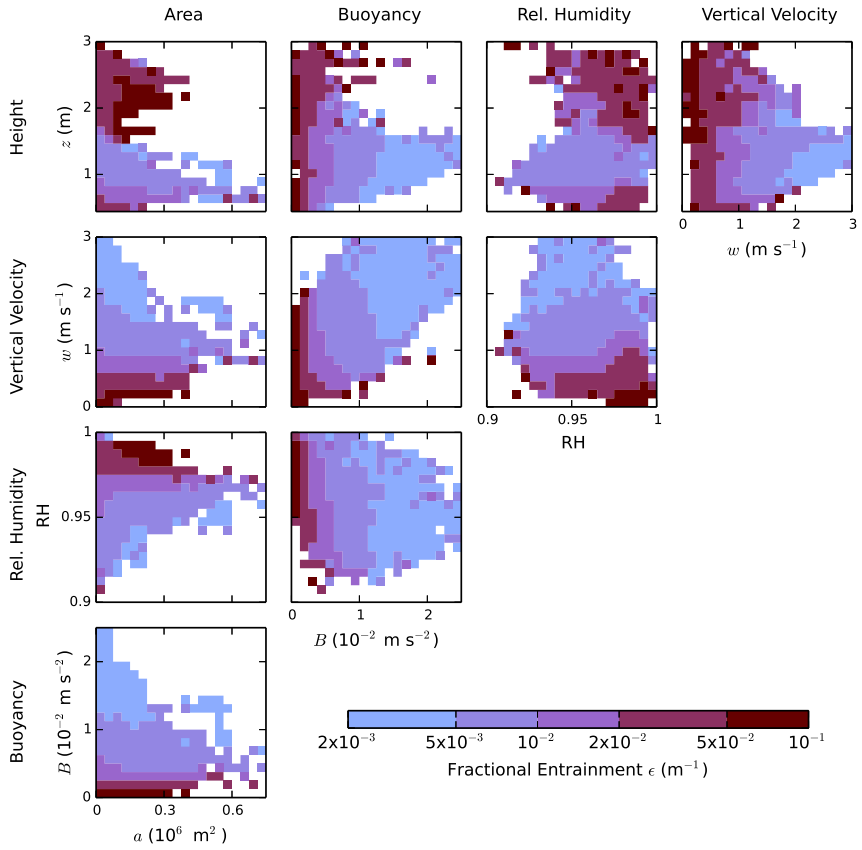

FIG. 3. Mean values of log10(ε) for each bin of joint probability density functions of various cloud core properties for individual clouds with thickness $d < 1000$ m in the CGILS output. The y axis of each row shows height, vertical velocity, relative humidity of the cloud shell, and buoyancy (from top to bottom), and the x axis of each column shows cross-sectional area, buoyancy, relative humidity of the cloud shell, and vertical velocity (from left to right).

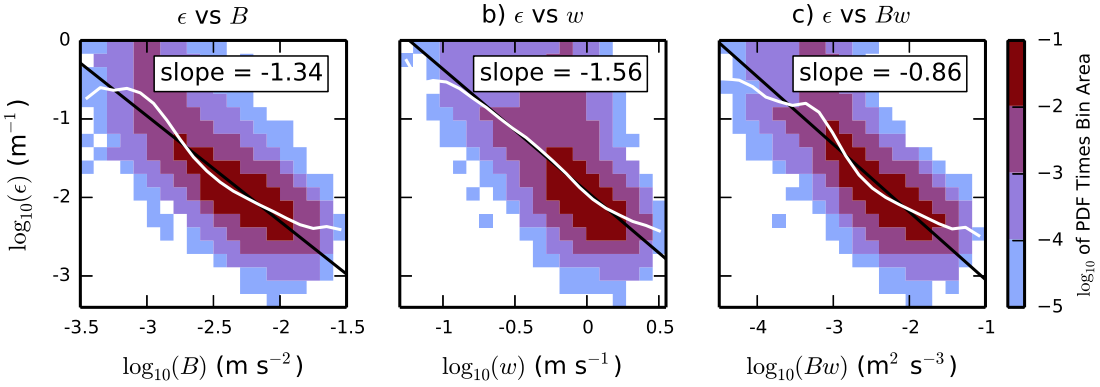

FIG. 4. Joint probability density functions multiplied by bin area ($P(x,y)\Delta x\Delta y$) for individual clouds with thickness $d < 1000$ m in the CGILS output of $\log_{10}(\varepsilon)$ versus (a) $\log_{10}$ of buoyancy, (b) $\log_{10}$ of vertical velocity, and (c) $\log_{10}$ of buoyancy times vertical velocity. PDFs are plotted using a logarithmic scale. White lines indicate the mean $\log_{10}(\varepsilon)$ value as a function of the x axis variable, and black lines show linear least-square best fits of $\log_{10}(\varepsilon)$ versus the x axis variable.